This article has been accepted for publication in a future issue of this journal, but has not been fully edited. Content may change prior to final publication. Citation information: DOI: 10.17775/CSEEJPES.2021.03680, CSEE Journal of Power and Energy Systems

A Least-Squares-Based Iterative Method with Better Convergence for PF/OPF of Integrated Transmission and Distribution Networks

Kunjie Tang, Shufeng Dong, Yonghua Song

***Abstract*—The limitations of the conventional master-slave-splitting (MSS) method, which is commonly applied to power flow and optimal power flow of integrated transmission and distribution networks (I-T&D), are analyzed first. Considering that the MSS suffers from a slow convergence rate or even divergence under some circumstances, a least-squares-based iterative (LSI) method is proposed. Compared with the MSS, the LSI modifies the iterative variables in each iteration by solving a least-squares problem with the information in previous iterations. Practical implementation and a parameter tuning strategy for the LSI are discussed. Further, a LSI-PF method is proposed to solve I-T&D power flow and a LSI-heterogeneous decomposition method (LSI-HGD) is proposed to solve optimal power flow. Numerical experiments demonstrate that the proposed LSI-PF and LSI-HGD methods can achieve the same accuracy as benchmark methods. Meanwhile, these LSI methods with appropriate settings significantly enhance the convergence and efficiency of conventional methods. Also, in some cases where conventional methods diverge, these LSI methods can still converge.**

***Index Terms*—integrated transmission and distribution networks, least-squares-based iterative method, fixed-point theory, master-slave-splitting method, power flow, optimal power flow.**

I. Introduction

With the high penetration of distributed energy resources, the coupling between transmission networks (TNs) and distribution networks (DNs) has been significantly enhanced [1]. Administration separation between transmission system operators (TSOs) and distribution system operators (DSOs) and physical coupling between TNs and DNs have gradually become contradictory in real-world operations. Under this background, the conventional separated and hierarchical analysis may lead to inaccurate results [2, 3].

To deal with this challenge, some countries have made specific plans for future operations to enhance the cooperation between TSOs and DSOs [4-6]. Meanwhile, some researchers also explore the coordinated analysis of integrated transmission-distribution networks (I-T&D) from different angles to provide theory basis and algorithm support, such as power flow (PF) [2, 7-10], contingency analysis [7, 11-13], optimal power flow (OPF) [3, 7, 14-19], etc. Reference [7] further establishes a generalized TN-DN coordinated model and proposes a generalized master-slave-splitting (MSS) method to solve this model with alternating iterations between TSOs and DSOs. The coordinated model and the MSS universally and effectively work for I-T&D PF, OPF, contingency analysis, voltage stability assessment, economic dispatch, etc. In essence, the mathematical foundation of them is the fixed-point theory, and the MSS is a specific application of the conventional fixed-point iterative method.

In recent years, some works further discuss how to improve the convergence of TN-DN alternating iterations and realize acceleration, since convergence is an important issue for an iterative method. For example, in I-T&D PF, [7] proposes a modified MSS with a distribution-response function, which is effective to make the algorithm converge faster. The loops in DNs usually degrades the convergence and efficiency of I-T&D PF calculation, and the modified MSS can handle this problem. Reference [9] presents a successive-intersection-approximation method to solve I-T&D PF. It can converge to accurate results under the cases where PV-typed and QV-typed distributed generations are accessed into DNs even if the MSS diverges under these cases. A rigorous proof shows that the method has a local quadratic convergence rate. In I-T&D OPF, [7] constructs a response function of a subsystem to reduce the derivative of the composite mapping of boundary variables, and thus, the overall convergence is enhanced. The response-function-based method is convenient, effective, and efficient in some circumstances, such as I-T&D PF and DC-model-based I-T&D OPF. Besides, some non-iterative methods are proposed to solve I-T&D OPF to avoid the potential divergence issue [18, 19]. However, these methods have some limitations: i) When the power injections at the root nodes of a DN is sensitive to their voltage magnitudes, the response-function-based method sometimes cannot guarantee the convergence; ii) When the model of a DN is complicated, e.g., nonconvex AC models, constructing an accurate response function is usually difficult since it involves some integral operations [7]; iii) Non-iterative methods usually sacrifice accuracy for higher efficiency.

One of the most important reasons for the bad convergence of conventional methods is that these methods are implemented with the simple fixed-point iteration, which indicates that the update iterative variables are only

This work was supported by the National Natural Science Foundation of China (52077193).

K. Tang and S. Dong (corresponding author) are with College of Electrical Engineering, Zhejiang University, Hangzhou, 310027 China (e-mail: tangkunjie1994@zju.edu.cn; dongshufeng@zju.edu.cn). Y. Song is with the State Key Laboratory of Internet of Things for Smart City and Department of Electrical and Computer Engineering, University of Macau, Macao SAR, China and also with the College of Electrical Engineering, Zhejiang University, Hangzhou 310027, China.

Citation information: DOI: 10.17775/CSEEJPES.2021.03680, CSEE Journal of Power and Energy Systems

determined by the information in the last iteration, regardless of the information in earlier iterations. To deal with this challenge, considering the features of I-T&D problems, some advanced derivative-free fixed-point iteration methods could be applied. The classical Krasnoselskii-Mann (KM) algorithm is helpful to enhance the convergence of the simple fixed-point iteration, but it usually suffers from a slower efficiency compared with the later methods [20, 21].

Therefore, this paper proposes a least-squares-based iterative (LSI) method to deal with I-T&D PF and OPF. The main contribution of the paper is that it:

i) analyzes the limitations of the MSS when it is applied in I-T&D PF and OPF based on the fixed-point theory;

ii) proposes a LSI with considerations about its practical implementation and convergence analysis;

iii) proposes a LSI-PF method to solve I-T&D PF;

iv) proposes a LSI-heterogeneous decomposition (LSI-HGD) method to solve I-T&D OPF;

The numerical experiment demonstrates that the proposed LSI-PF and LSI-HGD have better convergence and efficiency compared with conventional methods.

The rest of this paper is organized as follows. The conventional MSS and its limitations are discussed in Section II. Section III presents the LSI and its practical implementation. The LSI-PF and LSI-HGD methods for solving I-T&D PF and OPF are shown in Section IV. Numerical experiments are presented in Section V. Discussions and extensions are presented in Section VI. Finally, conclusions are drawn in Section VII.

II. Conventional MSS for I-T&D PF and OPF

This section will present the basic theory of the conventional MSS for I-T&D PF/OPF in Subsection A and analyze the limitations of this method in Subsection B based on the fixed-point theory.

A. Conventional MSS for I-T&D PF/OPF

Due to separate management and privacy issues, it is unreasonable to gather the data and models of TNs and DNs in a centralized manner to achieve an integrated system for analysis [2, 3]. Thus, a heterogeneous model is established, where TNs and DNs can be modeled with different approaches.

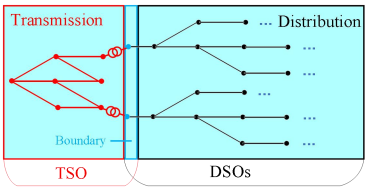

Fig. 1. Network partition of I-T&D

As shown in Fig. 1, one TN and multiple DNs are connected by several boundary buses. Thus, an I-T&D system can be divided into three parts: TN part, DN parts, and boundary part. The TSO usually manages the TN part while different DSOs usually manage different DN parts. The boundary part will be managed coordinately by both TSO and DSOs.

The MSS is proposed based on this heterogeneous model [2]. In specific, I-T&D PF and OPF can be modeled as a TSO subproblem and DSO subproblems as follows

$$\boldsymbol{x}=\boldsymbol{F}^{transm}(\boldsymbol{y}),\boldsymbol{F}^{transm}:\mathbf{R}^{n_2}\rightarrow\mathbf{R}^{n_1} \tag{1}$$

$$\boldsymbol{y}=\boldsymbol{F}^{distrib}(\boldsymbol{x}),\boldsymbol{F}^{distrib}:\mathbf{R}^{n_1}\rightarrow\mathbf{R}^{n_2} \tag{2}$$

where $\boldsymbol{x}$ represents the state variables of boundary nodes (voltage magnitude and angle, usually) and $\boldsymbol{y}$ represents the active and reactive power injections at boundary nodes. n_1 is the dimension of $\boldsymbol{x}$ and n_2 is the dimension of $\boldsymbol{y}$. $\boldsymbol{F}^{transm}$ denotes an abstract mapping of TSO, representing that $\boldsymbol{x}$ will be achieved if the TSO subproblem is solved with the variables $\boldsymbol{y}$. $\boldsymbol{F}^{distrib}$ denotes an abstract mapping of DSOs, representing that $\boldsymbol{y}$ will be achieved if the DSO subproblems are solved with the variables $\boldsymbol{x}$. The goal of solving an I-T&D problem is to find $\boldsymbol{x}^*$ such that [2, 3]

$$\boldsymbol{x}^*=\boldsymbol{F}^{transm}(\boldsymbol{F}^{distrib}(\boldsymbol{x}^*)),\boldsymbol{F}^{transm}(\boldsymbol{F}^{distrib}(\bullet)):\mathbf{R}^{n_1}\rightarrow\mathbf{R}^{n_1} \tag{3}$$

Here, $\boldsymbol{x}^*\in\mathbf{R}^{n_1}$ is the fixed point of the composite mapping $\boldsymbol{F}^{transm}(\boldsymbol{F}^{distrib}(\bullet))$, denoted as $\boldsymbol{f}(\bullet)$.

The standard implementation of the conventional MSS is a simple fixed-point iteration in essence. Given an initial value $\boldsymbol{x}_0$ of boundary state variables, the final solution will be achieved with

$$\boldsymbol{x}_{k+1}=\boldsymbol{F}^{transm}(\boldsymbol{F}^{distrib}(\boldsymbol{x}_k))=\boldsymbol{f}(\boldsymbol{x}_k),k=0,1,2,\cdots \tag{4}$$

Particularly, when solving I-T&D OPF, the MSS is also called the HGD method [3].

B. Limitations of Conventional MSS

According to the convergence condition of the fixed-point theory, the conventional MSS may diverge or suffer from oscillations if [2]

$$\rho\left(\frac{\partial \boldsymbol{f}}{\partial \boldsymbol{x}}\right)\geq 1 \tag{5}$$

where $\rho(\cdot)$ represents the spectral radius.

In I-T&D PF, for example, [9] points out that, when the power injections at boundary nodes are sensitive to the voltage magnitude of boundary nodes, the MSS may diverge. For example, the penetration of PV-typed distributed generations (DGs) and heavy loads in DNs may both lead to this problem. The numerical experiments in [9] also demonstrate this point.

In I-T&D OPF, Case E is used to illustrate this point. The detailed information of Case E is shown in TABLE B-III in Appendix B. Fig. 2 compares the voltage magnitude of a boundary node (Bus No. 11) in this case under the MSS (HGD) and a centralized method. It clearly shows that the voltage magnitude of the boundary node is deterministic under the centralized method. However, under the MSS (HGD), the voltage magnitude of the boundary node fluctuates around the accurate value and cannot converge within finite iterations.

Citation information: DOI: 10.17775/CSEEJPES.2021.03680, CSEE Journal of Power and Energy Systems

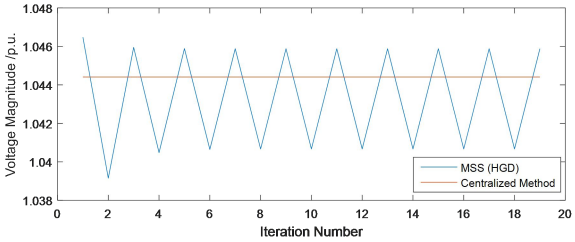

Fig. 2. Voltage magnitude of a boundary node

III. LSI and Its Practical Implementation

In this section, Subsection A presents the basic theory of the LSI. Subsection B gives its detailed steps. Convergence analysis is shown in Subsection C and parameter tuning is discussed in Subsection D, finally.

A. LSI

As mentioned in Section II-B, the conventional MSS may suffer from slow convergence or divergence in some circumstances. To deal with this challenge, a method of successive approximations on boundary iterative variables could be applied. A conventional method is the KM iteration method [20, 21]. In each iteration of this method, each boundary variable is modified with the mean value in two previous iterations. The effect of this method may not be significant for two reasons: i) only the historical data of the two previous iterations is used to modify boundary variables; ii) take the mean value may not achieve the best effect of improving convergence sometimes.

Thus, this paper extends and generalizes the conventional methods of successive approximations into a LSI. The LSI is a variant of the conventional fixed-point iteration. The basic theory of the LSI is as follows.

Define $\boldsymbol{g}:\boldsymbol{D}\subset\mathbf{R}^n\to\mathbf{R}^n$,

$$\boldsymbol{g}(\boldsymbol{x})=\boldsymbol{x}-\boldsymbol{f}(\boldsymbol{x}) \tag{6}$$

Thus, in the k-th iteration, a least-squares problem (7) with a normalization constraint will be solved

$$\min\left\|\sum_{j=0}^{m_k}\alpha_j\boldsymbol{g}(\boldsymbol{x}_{k-m_k+j})\right\|_2^2 \quad s.t.\sum_{j=0}^{m_k}\alpha_j=1 \tag{7}$$

where m_k is determined as (8), given a user-defined constant m

$$m_k=\min\{m,k\} \tag{8}$$

and the vector $\boldsymbol{\alpha}^k=(\alpha_0^k,\cdots,\alpha_{m_k}^k)$ will be achieved.

Here, m represents a size, which indicates that the results of at most m previous iterations are used to modify the values of iteration variables in each iteration. Then,

$$\boldsymbol{x}_{k+1}=\sum_{j=0}^{m_k}\alpha_j^k\boldsymbol{f}(\boldsymbol{x}_{k-m_k+j}) \tag{9}$$

As shown in (6)-(9), the LSI is a generalized form of the conventional KM iteration method. On the one hand, a user-defined m is introduced into the method, which indicates that more historical data may be used to modify boundary variables in each iteration. On the other hand, solving a least-squares problem in each iteration minimizes the residual error, which achieves a better effect than taking the mean value.

B. Detailed Steps

As shown in Subsection A, one constrained least-squares problem (7) needs to be solved in each iteration. Admittedly, it is feasible to solve this problem with mature solvers for solving convex optimization problems. However, it is more time-consuming compared with simple matrix operations. Thus, a more efficient method is proposed. Since the minimization problem (7) can be efficiently solved as an unconstrained least squares problem by a variable elimination, reformulate (7) as

$$\min_{\boldsymbol{\gamma}}\left\|\boldsymbol{g}_k-\boldsymbol{Y}_k\boldsymbol{\gamma}\right\|_2 \tag{10}$$

where $\boldsymbol{\gamma}=(\gamma_0,\cdots,\gamma_{m_k-1})$, $\boldsymbol{g}_k=\boldsymbol{g}(\boldsymbol{x}_k)$, $\boldsymbol{Y}_k=\left[\boldsymbol{y}_{k-m_k}\cdots\boldsymbol{y}_{k-1}\right]$ with $\boldsymbol{y}_i=\boldsymbol{g}_{i+1}-\boldsymbol{g}_i$ for $0\le i\le m_k-1$. Thus,

$$\begin{cases}\boldsymbol{\alpha}_i=\boldsymbol{\gamma}_0, i=0\\ \boldsymbol{\alpha}_i=\boldsymbol{\gamma}_{i+1}-\boldsymbol{\gamma}_i, 1\le i<m_k-1\\ \boldsymbol{\alpha}_i=1-\boldsymbol{\gamma}_{m_k-1}, i=m_k-1\end{cases} \tag{11}$$

When $\boldsymbol{Y}_k$ is full column rank, the solution $\boldsymbol{\gamma}_k$ to (10) is

$$\boldsymbol{\gamma}_k=(\boldsymbol{Y}_k^{\mathrm{T}}\boldsymbol{Y}_k)^{-1}\boldsymbol{Y}_k^{\mathrm{T}}\boldsymbol{g}_k \tag{12}$$

Thus,

$$\begin{aligned}\boldsymbol{x}_{k+1}&=\boldsymbol{f}(\boldsymbol{x}_k)-\sum_{i=0}^{m_k-1}\gamma_i^k[\boldsymbol{f}(\boldsymbol{x}_{k-m_k+i+1})-\boldsymbol{f}(\boldsymbol{x}_{k-m_k+i})]\\&=\boldsymbol{f}(\boldsymbol{x}_k)-(\boldsymbol{S}_k-\boldsymbol{Y}_k)(\boldsymbol{Y}_k^{\mathrm{T}}\boldsymbol{Y}_k)^{-1}\boldsymbol{Y}_k^{\mathrm{T}}\boldsymbol{g}_k\end{aligned} \tag{13}$$

where $\boldsymbol{S}_k=\left[\boldsymbol{s}_{k-m_k}\quad\cdots\quad\boldsymbol{s}_{k-1}\right]$ with $\boldsymbol{s}_i=\boldsymbol{x}_{i+1}-\boldsymbol{x}_i$ for each i.

Based on (13), the detailed steps are as follows.

Step 1: Initialize $\boldsymbol{x}_0$, ε, m, $\boldsymbol{S}_0$, and $\boldsymbol{Y}_0$, where ε is the convergence tolerance; $\boldsymbol{S}_0$ and $\boldsymbol{Y}_0$ are empty matrices. Let iteration count $k=0$.

Step 2: According to (13), calculate $\boldsymbol{x}_{k+1}$ as

$$\boldsymbol{x}_{k+1}=\begin{cases}\boldsymbol{f}(\boldsymbol{x}_k), k=0\\ \boldsymbol{f}(\boldsymbol{x}_k)-(\boldsymbol{S}_k-\boldsymbol{Y}_k)(\boldsymbol{Y}_k^{\mathrm{T}}\boldsymbol{Y}_k)^{-1}\boldsymbol{Y}_k^{\mathrm{T}}\boldsymbol{g}_k, k\ge1\end{cases} \tag{14}$$

Step 3: If $\left\|\boldsymbol{x}_{k+1}-\boldsymbol{x}_k\right\|<\varepsilon$, the LSI converges and stops, otherwise, go to **Step 4**.

Step 4: If $k<m$, calculate $\boldsymbol{S}_{k+1}$ and $\boldsymbol{Y}_{k+1}$ as

$$\boldsymbol{S}_{k+1}\leftarrow\left[\boldsymbol{S}_k\quad\boldsymbol{x}_{k+1}-\boldsymbol{x}_k\right] \tag{15}$$

$$\boldsymbol{Y}_{k+1}\leftarrow\left[\boldsymbol{Y}_k\quad\boldsymbol{x}_{k+1}-\boldsymbol{f}(\boldsymbol{x}_{k+1})-\boldsymbol{g}(\boldsymbol{x}_k)\right] \tag{16}$$

Otherwise,

$$\boldsymbol{S}_{k+1}\leftarrow\left[\boldsymbol{S}_k\begin{bmatrix}\boldsymbol{0}\\ \boldsymbol{I}\end{bmatrix}\quad\boldsymbol{x}_{k+1}-\boldsymbol{x}_k\right] \tag{17}$$

Citation information: DOI: 10.17775/CSEEJPES.2021.03680, CSEE Journal of Power and Energy Systems

$$\boldsymbol{Y}_{k+1} \leftarrow \left[\boldsymbol{Y}_k \begin{bmatrix} \boldsymbol{0} \\ \boldsymbol{I} \end{bmatrix} \quad \boldsymbol{x}_{k+1} - \boldsymbol{f}(\boldsymbol{x}_{k+1}) - \boldsymbol{g}(\boldsymbol{x}_k) \right] \tag{18}$$

where $\boldsymbol{I}$ represents an identity matrix, of which the dimension is $m-1$. The essence of (17) and (18) is to eliminate the first column of $\boldsymbol{S}_{k+1}$ and $\boldsymbol{Y}_{k+1}$. Then, add a new column, calculated with the updated iteration variables, as the last column.

Step 5: Let $k \leftarrow k+1$ and go to **Step 2**.

C. Convergence Analysis

To analyze the convergence of the LSI, some assumptions are established as follows.

i) There exists $\boldsymbol{x}^*$ such that

$$\boldsymbol{g}(\boldsymbol{x}^*) = \boldsymbol{x}^* - \boldsymbol{f}(\boldsymbol{x}^*) = \boldsymbol{0} \tag{19}$$

ii) $\boldsymbol{f}$ is Lipschitz continuously differentiable in the ball $\boldsymbol{B}(\hat{\rho}) = \{\boldsymbol{x} \,|\, \|\boldsymbol{e}\| \le \hat{\rho}\}$ for some $\rho > 0$, where

$$\boldsymbol{e} = \boldsymbol{x} - \boldsymbol{x}^* \tag{20}$$

iii) There exists $c \in (0,1)$ such that for all $\boldsymbol{u}, \boldsymbol{v} \in \boldsymbol{B}(\hat{\rho})$,

$$\|\boldsymbol{f}(\boldsymbol{u}) - \boldsymbol{f}(\boldsymbol{v})\| \le c\|\boldsymbol{u} - \boldsymbol{v}\| \tag{21}$$

iv) There is M_α such that for all $k \ge 0$,

$$\sum_{j=0}^{m_k} |\alpha_j| \le M_\alpha \tag{22}$$

Here, it is assumed that all these prerequisites are satisfied in I-T&D PF and I-T&D OPF. These assumptions are weak, which implies common assumptions for local convergence of Newton's method. Thus, these assumptions will not severely jeopardize the generality of the convergence analysis. With these assumptions, Theorem 1 is established.

Theorem 1 Let Assumptions i)-iv) hold and $c < \hat{c} < 1$. If $\boldsymbol{x}^0$ is sufficiently close to $\boldsymbol{x}^*$, the LSI converges to $\boldsymbol{x}^*$ as

$$\|\boldsymbol{g}(\boldsymbol{x}_k)\| \le \hat{c}^k \|\boldsymbol{g}(\boldsymbol{x}_0)\| \tag{23}$$

Theorem 1 is proved by induction in Appendix A. Note that Theorem 1 gives a sufficient convergence condition, which is useful for proving the convergence theoretically. Thus, even if some assumptions are not satisfied, the LSI may still converge in the practical implementation.

D. Parameter Tuning

As shown in Subsection A and B, m is an important user-defined constant, which has a significant influence on the overall efficiency of the LSI. If m is too small, the storage information used by the method may be too limited to provide fast convergence. While if m is too large, the least-squares problem may be seriously ill-conditioned. Also, outdated information from previous iterations may jeopardize the convergence of the method.

Generally, it is hard to give a rigorous strategy for parameter tuning of the LSI, and the best choice of m is application-dependent. However, it is unnecessary to tune the value of m for each system. According to numerical experiments, m = 3 is usually a proper empirical setting for most applications. The proposed methods have good performance under this setting.

IV. LSI-Based Methods for I-T&D PF and OPF

In this section, Subsection A proposes the LSI-PF method. Subsection B proposes the LSI-HGD method. Subsection C finally presents the data flow between TSO and DSOs.

A. LSI-PF Method for I-T&D PF

The goal of I-T&D PF is to solve the equations [2]

$$\begin{cases} \boldsymbol{f}^{transm}(\boldsymbol{V}^{transm}, \boldsymbol{\theta}^{transm}, \boldsymbol{V}^B, \boldsymbol{\theta}^B) = \boldsymbol{0} \\ \boldsymbol{f}_P^B(\boldsymbol{V}^{transm}, \boldsymbol{\theta}^{transm}, \boldsymbol{V}^B, \boldsymbol{\theta}^B) = \boldsymbol{P}^B \\ \boldsymbol{f}_Q^B(\boldsymbol{V}^{transm}, \boldsymbol{\theta}^{transm}, \boldsymbol{V}^B, \boldsymbol{\theta}^B) = \boldsymbol{Q}^B \end{cases} \tag{24}$$

$$\boldsymbol{f}^{distrib}(\boldsymbol{V}^{distrib}, \boldsymbol{\theta}^{distrib}, \boldsymbol{V}^B, \boldsymbol{\theta}^B) = \boldsymbol{0} \tag{25}$$

where $\boldsymbol{P}^B$ and $\boldsymbol{Q}^B$ represent the active and reactive power injections at boundary nodes; $\boldsymbol{V}^B$ and $\boldsymbol{\theta}^B$ represent the voltage magnitude and angle of boundary nodes. $\boldsymbol{f}$ represents the power flow equations. The superscripts '*transm*', '*distrib*', and '*B*' represent the TN part, DN part, and boundary part. Particularly, $\boldsymbol{f}_P^B = \boldsymbol{P}^B$ and $\boldsymbol{f}_Q^B = \boldsymbol{Q}^B$ respectively represent the boundary power flow equations of active power and reactive power.

In I-T&D PF, TSO sends $\boldsymbol{V}^B$ and $\boldsymbol{\theta}^B$ to DSOs while DSOs send $\boldsymbol{P}^B$ and $\boldsymbol{Q}^B$ to TSO. Thus, let

$$\boldsymbol{x} = \left[\boldsymbol{V}^B; \boldsymbol{\theta}^B\right], \boldsymbol{y} = \left[\boldsymbol{P}^B; \boldsymbol{Q}^B\right] \tag{26}$$

Thus, based on (4) and (5), $\boldsymbol{F}^{transm}$ represents TN power flow, where the power injections at boundary nodes are given and the voltage magnitude and angle of boundary nodes are solved. Similarly, $\boldsymbol{F}^{distrib}$ represents DN power flow, where the voltage magnitude and angle of boundary nodes are given and the power injections at boundary nodes are solved. According to the LSI presented in Section III, a LSI-PF method could be achieved as follows:

Step 1: Initialize $\boldsymbol{x}_0$, ε, m, $\boldsymbol{S}_0$, and $\boldsymbol{Y}_0$, where ε is the convergence tolerance; $\boldsymbol{S}_0$ and $\boldsymbol{Y}_0$ are empty matrices. Let iteration count $k = 0$.

Step 2: DSOs solve the DN power flow with $\boldsymbol{x}_k$ to achieve $\boldsymbol{y}_k$ and send $\boldsymbol{y}_k$ to TSO. Then, TSO solves the TN power flow with $\boldsymbol{y}_k$ to achieve $\hat{\boldsymbol{x}}_{k+1}$. Calculates $\boldsymbol{x}_{k+1}$ as

$$\boldsymbol{x}_{k+1} = \begin{cases} \hat{\boldsymbol{x}}_{k+1}, k = 0 \\ \hat{\boldsymbol{x}}_{k+1} - (\boldsymbol{S}_k - \boldsymbol{Y}_k)(\boldsymbol{Y}_k^{\mathrm{T}}\boldsymbol{Y}_k)^{-1}\boldsymbol{Y}_k^{\mathrm{T}}\boldsymbol{g}_k, k \ge 1 \end{cases} \tag{27}$$

Step 3: If $\|\boldsymbol{x}_{k+1} - \boldsymbol{x}_k\| < \varepsilon$, the LSI-PF converges and stops, otherwise, go to **Step 4**.

Step 4: TSO sends $\boldsymbol{x}_{k+1}$ to DSOs. DSOs solve the DN power flow with $\boldsymbol{x}_{k+1}$ to achieve $\boldsymbol{y}_{k+1}$ and send $\boldsymbol{y}_{k+1}$ to TSO. Then TSO solves the TN power flow with $\boldsymbol{y}_{k+1}$ to achieve

Citation information: DOI: 10.17775/CSEEJPES.2021.03680, CSEE Journal of Power and Energy Systems

$\hat{\boldsymbol{x}}_{k+2}$. If $k < m$, calculate $\boldsymbol{S}_{k+1}$ and $\boldsymbol{Y}_{k+1}$ as

$$\boldsymbol{S}_{k+1} \leftarrow \left[\boldsymbol{S}_k \quad \boldsymbol{x}_{k+1} - \boldsymbol{x}_k\right] \tag{28}$$

$$\boldsymbol{Y}_{k+1} \leftarrow \left[\boldsymbol{Y}_k \quad \boldsymbol{x}_{k+1} - \hat{\boldsymbol{x}}_{k+2} - (\boldsymbol{x}_k - \hat{\boldsymbol{x}}_{k+1})\right] \tag{29}$$

Otherwise,

$$\boldsymbol{S}_{k+1} \leftarrow \left[\boldsymbol{S}_k \begin{bmatrix}\boldsymbol{0}\\ \boldsymbol{I}\end{bmatrix} \quad \boldsymbol{x}_{k+1} - \boldsymbol{x}_k\right] \tag{30}$$

$$\boldsymbol{Y}_{k+1} \leftarrow \left[\boldsymbol{Y}_k \begin{bmatrix}\boldsymbol{0}\\ \boldsymbol{I}\end{bmatrix} \quad \boldsymbol{x}_{k+1} - \hat{\boldsymbol{x}}_{k+2} - (\boldsymbol{x}_k - \hat{\boldsymbol{x}}_{k+1})\right] \tag{31}$$

Step 5: Let $k \leftarrow k+1$ and go to **Step 2**.

B. LSI-HGD Method for I-T&D OPF

In I-T&D OPF, the goal of I-T&D OPF is to solve [3]

$$\begin{aligned}&\min_{\substack{\boldsymbol{u}^{transm},\boldsymbol{u}^{B},\boldsymbol{u}^{distrib},\\ \boldsymbol{V}^{transm},\boldsymbol{V}^{B},\boldsymbol{V}^{distrib},\\ \boldsymbol{\theta}^{transm},\boldsymbol{\theta}^{B},\boldsymbol{\theta}^{distrib}}} c^{transm}(\boldsymbol{u}^{transm},\boldsymbol{u}^{B},\boldsymbol{V}^{transm},\boldsymbol{\theta}^{transm},\boldsymbol{V}^{B},\boldsymbol{\theta}^{B})\\ &+c^{distrib}(\boldsymbol{u}^{distrib},\boldsymbol{V}^{distrib},\boldsymbol{\theta}^{distrib},\boldsymbol{V}^{B},\boldsymbol{\theta}^{B})\end{aligned} \tag{32}$$

under a series of constraints, where $\boldsymbol{u}$ represents control variables, such as the active and reactive output of generators and distributed generations. c represents the cost function. The superscripts '*transm*', '*distrib*', and '*B*' represent the TN part, DN part, and boundary part.

Considering the privacy issues, (32) could be decoupled into DSO subproblems (33) and a TSO subproblem (34) with optimal condition decomposition and boundary data exchange based on the HGD [3].

$$\begin{aligned}&\min_{\substack{\boldsymbol{u}^{distrib},\boldsymbol{V}^{distrib},\\ \boldsymbol{\theta}^{distrib},\boldsymbol{P}^{B},\boldsymbol{Q}^{B}}} c^{distrib}(\boldsymbol{u}^{distrib},\boldsymbol{V}^{distrib},\boldsymbol{\theta}^{distrib},\boldsymbol{V}^{B}_{transm},\boldsymbol{\theta}^{B}_{transm})+c_{auxD}\\ &s.t.\ \ (\boldsymbol{u}^{distrib},\boldsymbol{V}^{distrib},\boldsymbol{\theta}^{distrib},\boldsymbol{P}^{B},\boldsymbol{Q}^{B})\in\Omega^{distrib}(\boldsymbol{V}^{B}_{transm},\boldsymbol{\theta}^{B}_{transm})\end{aligned} \tag{33}$$

$$\begin{aligned}&\min_{\substack{\boldsymbol{u}^{trnasm},\boldsymbol{V}^{transm},\\ \boldsymbol{\theta}^{transm},\boldsymbol{u}^{B},\boldsymbol{V}^{B},\boldsymbol{\theta}^{B}}} c^{transm}(\boldsymbol{u}^{transm},\boldsymbol{u}^{B},\boldsymbol{V}^{transm},\boldsymbol{\theta}^{transm},\boldsymbol{V}^{B},\boldsymbol{\theta}^{B})+c_{auxT}\\ &s.t.\ \ (\boldsymbol{u}^{transm},\boldsymbol{u}^{B},\boldsymbol{V}^{transm},\boldsymbol{\theta}^{transm},\boldsymbol{V}^{B},\boldsymbol{\theta}^{B})\in\Omega^{transm}(\boldsymbol{P}^{B}_{distrib},\boldsymbol{Q}^{B}_{distrib})\end{aligned} \tag{34}$$

where $\Omega^{distrib}$ and Ω^{transm} represent the feasible regions of DSO and TSO subproblems, respectively. $\boldsymbol{V}^{B}_{transm}$ and $\boldsymbol{\theta}^{B}_{transm}$ represent the optimization results of $\boldsymbol{V}^{B}$ and $\boldsymbol{\theta}^{B}$ by solving the TSO subproblem. $\boldsymbol{P}^{B}_{distrib}$ and $\boldsymbol{Q}^{B}_{distrib}$ represent the optimization results of $\boldsymbol{P}^{B}$ and $\boldsymbol{Q}^{B}$ by solving the DSO subproblems. c_{auxT} and c_{auxD} are two auxiliary functions, which are introduced to ensure the optimality conditions of the model [3].

To present more details about these two auxiliary functions, (33) and (34) are rewritten as a more detailed form.

$$\begin{aligned}&\min_{\boldsymbol{u}^{distrib},\boldsymbol{V}^{distrib},\boldsymbol{\theta}^{distrib}} c^{distrib}(\boldsymbol{u}^{distrib},\boldsymbol{V}^{distrib},\boldsymbol{\theta}^{distrib},\boldsymbol{V}^{B}_{transm},\boldsymbol{\theta}^{B}_{transm})+c_{auxD}\\ &s.t.\ \ \boldsymbol{f}^{distrib}(\boldsymbol{V}^{B}_{transm},\boldsymbol{\theta}^{B}_{transm},\boldsymbol{u}^{distrib},\boldsymbol{V}^{distrib},\boldsymbol{\theta}^{distrib})=\boldsymbol{0}:\boldsymbol{\lambda}_{distrib}\\ &\quad\ \boldsymbol{g}^{distrib}(\boldsymbol{V}^{B}_{transm},\boldsymbol{\theta}^{B}_{transm},\boldsymbol{u}^{distrib},\boldsymbol{V}^{distrib},\boldsymbol{\theta}^{distrib})\ge\boldsymbol{0}:\boldsymbol{\mu}_{distrib}\\ &\begin{bmatrix}\boldsymbol{P}^{B}\\ \boldsymbol{Q}^{B}\end{bmatrix}=\boldsymbol{f}^{B-distrib}(\boldsymbol{V}^{B}_{transm},\boldsymbol{\theta}^{B}_{transm},\boldsymbol{u}^{distrib},\boldsymbol{V}^{distrib},\boldsymbol{\theta}^{distrib}):\boldsymbol{\lambda}_{B-distrib}\end{aligned} \tag{35}$$

$$\begin{aligned}&\min_{\substack{\boldsymbol{u}^{trnasm},\boldsymbol{V}^{transm},\\ \boldsymbol{\theta}^{transm},\boldsymbol{u}^{B},\boldsymbol{V}^{B},\boldsymbol{\theta}^{B}}} c^{transm}(\boldsymbol{u}^{transm},\boldsymbol{u}^{B},\boldsymbol{V}^{transm},\boldsymbol{\theta}^{transm},\boldsymbol{V}^{B},\boldsymbol{\theta}^{B})+c_{auxT}\\ &s.t.\ \ \boldsymbol{f}^{transm}(\boldsymbol{u}^{transm},\boldsymbol{u}^{B},\boldsymbol{V}^{transm},\boldsymbol{\theta}^{transm},\boldsymbol{V}^{B},\boldsymbol{\theta}^{B})=\boldsymbol{0}:\boldsymbol{\lambda}_{transm}\\ &\quad\ \boldsymbol{g}^{transm}(\boldsymbol{u}^{transm},\boldsymbol{u}^{B},\boldsymbol{V}^{transm},\boldsymbol{\theta}^{transm},\boldsymbol{V}^{B},\boldsymbol{\theta}^{B})\ge\boldsymbol{0}:\boldsymbol{\mu}_{transm}\\ &\boldsymbol{f}^{transm-B}(\boldsymbol{u}^{transm},\boldsymbol{u}^{B},\boldsymbol{V}^{transm},\boldsymbol{\theta}^{transm},\boldsymbol{V}^{B},\boldsymbol{\theta}^{B})=\begin{bmatrix}\boldsymbol{P}^{B}_{distrib}\\ \boldsymbol{Q}^{B}_{distrib}\end{bmatrix}:\boldsymbol{\lambda}_{transm-B}\end{aligned} \tag{36}$$

where $\boldsymbol{f}$ and $\boldsymbol{g}$ represent equality and inequality constraints, respectively; $\boldsymbol{\lambda}$ and $\boldsymbol{\mu}$ represent Lagrange multipliers. Particularly, the subscripts '*B-distrib*' and '*transm-B*' respectively represent the boundary power flow constraints in the DSO subproblem and the TSO subproblem.

Thus, the two auxiliary functions can be calculated as

$$c_{auxT} = (\boldsymbol{h}^{B})^{\mathrm{T}}\begin{bmatrix}\boldsymbol{V}^{B}\\ \boldsymbol{\theta}^{B}\end{bmatrix} \tag{37}$$

$$c_{auxD} = \boldsymbol{\lambda}^{\mathrm{T}}_{transm-B}\begin{bmatrix}\boldsymbol{P}^{B}\\ \boldsymbol{Q}^{B}\end{bmatrix} \tag{38}$$

where [3]

$$\begin{aligned}\boldsymbol{h}_B = &\frac{\partial c^{distrib}}{\partial[\boldsymbol{V}^{B};\boldsymbol{\theta}^{B}]}-\boldsymbol{\lambda}^{\mathrm{T}}_{distrib}\frac{\partial \boldsymbol{f}^{distrib}}{\partial[\boldsymbol{V}^{B};\boldsymbol{\theta}^{B}]}\\ &-\boldsymbol{\mu}^{\mathrm{T}}_{distrib}\frac{\partial \boldsymbol{g}^{distrib}}{\partial[\boldsymbol{V}^{B};\boldsymbol{\theta}^{B}]}+\boldsymbol{\lambda}^{\mathrm{T}}_{B-distrib}\frac{\partial \boldsymbol{f}^{B-distrib}}{\partial[\boldsymbol{V}^{B};\boldsymbol{\theta}^{B}]}\end{aligned} \tag{39}$$

In I-T&D OPF, TSO sends $\boldsymbol{V}^{B}$, $\boldsymbol{\theta}^{B}$, and $\boldsymbol{\lambda}_{B\text{-}distrib}$ to DSOs while DSOs send $\boldsymbol{h}^{B}$, $\boldsymbol{P}^{B}$, and $\boldsymbol{Q}^{B}$ to TSO. Thus, let

$$\boldsymbol{x}=\left[\boldsymbol{V}^{B};\boldsymbol{\theta}^{B};\boldsymbol{\lambda}^{B}\right],\boldsymbol{y}=\left[\boldsymbol{P}^{B};\boldsymbol{Q}^{B};\boldsymbol{h}^{B}\right] \tag{40}$$

Thus, based on (4) and (5), $\boldsymbol{F}^{transm}$ represents the TSO subproblem, where the power injections at boundary nodes, as well as $\boldsymbol{h}^{B}$, are given and the voltage magnitude and angle of boundary nodes, as well as λ^{B}, are achieved. Similarly, $\boldsymbol{F}^{distrib}$ represents the DSO subproblems, where the voltage magnitude and angle of boundary nodes, as well as λ^{B}, are given and the power injections at boundary nodes are, as well as $\boldsymbol{h}^{B}$, solved. According to the LSI presented in Section III, a LSI-HGD method could be achieved as follows:

Step 1: Initialize $\boldsymbol{x}_0$, ε, m, $\boldsymbol{S}_0$, and $\boldsymbol{Y}_0$, where ε is the convergence tolerance; $\boldsymbol{S}_0$ and $\boldsymbol{Y}_0$ are empty matrices. Let iteration count $k = 0$.

Step 2: DSOs solve the DSO subproblems with $\boldsymbol{x}_k$ to achieve $\boldsymbol{y}_k$ and send $\boldsymbol{y}_k$ to TSO. Then, TSO solves the TSO

Citation information: DOI: 10.17775/CSEEJPES.2021.03680, CSEE Journal of Power and Energy Systems

subproblem with $\boldsymbol{y}_k$ to achieve $\hat{\boldsymbol{x}}_{k+1}$. Calculates $\boldsymbol{x}_{k+1}$ as (27).

Step 3: If $\|\boldsymbol{x}_{k+1}-\boldsymbol{x}_k\|<\varepsilon$, the LSI-HGD converges and stops, otherwise, go to **Step 4**.

Step 4: TSO sends $\boldsymbol{x}_{k+1}$ to DSOs. DSOs solve the DSO subproblem with $\boldsymbol{x}_{k+1}$ to achieve $\boldsymbol{y}_{k+1}$ and send $\boldsymbol{y}_{k+1}$ to TSO. Then TSO solves the TSO subproblem with $\boldsymbol{y}_{k+1}$ to achieve $\hat{\boldsymbol{x}}_{k+2}$. If $k<m$, calculate $\boldsymbol{S}_{k+1}$ and $\boldsymbol{Y}_{k+1}$ as (28) and (29). Otherwise, calculate $\boldsymbol{S}_{k+1}$ and $\boldsymbol{Y}_{k+1}$ as (30) and (31).

Step 5: Let $k \leftarrow k+1$ and go to **Step 2**.

C. TSO-DSO Data Flow

Detailed steps and data flow between TSO and DSOs in the LSI-PF and LSI-HGD are shown in Fig. 3.

It clearly shows that TSO and DSOs only need to exchange boundary information, which will not lead to a heavy communication burden. Also, in this way, the privacies of TSO and DSOs are both well-protected.

Besides, the proposed LSI-based methods does not increase TSO-DSO communication compared with the conventional I-T&D PF and OPF methods, since it also solves $\boldsymbol{f}(\boldsymbol{x})$ only once for each iteration.

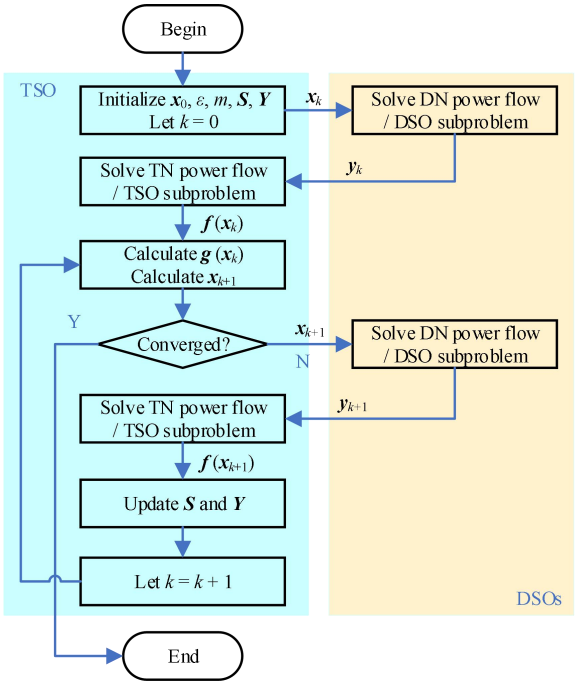

Fig. 3. Steps and data flow of the LSI-PF and LSI-HGD

V. Numerical Experiments

The programs for the test are written in MATLAB R2019a and run on the Windows 10 of 64 bits. The CPU is Intel Core i7-7700K, with 4.20GHz master frequency and 32GB memory. Several I-T&D cases are constructed, of which the detailed information is shown in Appendix B.

A. LSI-PF for I-T&D PF

Three I-T&D PF methods are investigated: i) Centralized Newton-based PF (C-PF): unrealistic in real-world operation, it is an accurate model, which can be considered as a benchmark in the test. The algorithm applied in the test is the 'runpf' function in MATPOWER 7.0; ii) MSS method (MSS-PF) [2]; iii) the LSI-based I-T&D PF (LSI-PF). The convergence tolerance is set as 1e-6. The flat start is applied for initial value selection, i.e., the initial values of boundary nodal voltage magnitudes are 1 p.u. and the initial values of boundary nodal voltage angles are 0°. The maximum iteration number between TSO and DSOs for ii) and iii) is set as 100.

TABLE I records the voltage magnitudes and angles of boundary nodes in some cases. It shows that, under Case A and C, the LSI-PF can achieve the same results as the C-PF and the MSS-PF. Under Case B and D, the conventional MSS-PF diverges, while the LSI-PF can still achieve the same results as the C-PF.

TABLE II records the iterations and time consumptions under different algorithms. It shows that the LSI-PF can converge under all cases while the MSS-PF diverges under Case B and D. Further, for most cases, the LSI-PF can improve the convergence rate and take fewer iterations to converge. Here, in Cases A-D, DGs in DNs are controlled with PV mode while they are controlled in QV mode in Cases A2-D2, which indicates that the proposed LSI-PF has good adaptability to different control modes of DGs. The value of m is closely related to the convergence rate and efficiency of the algorithm. Generally, $m \geq 3$ can achieve a satisfying result.

TABLE I
I-T&D PF Results under Different Algorithms

Case	Boundary Node No.	Voltage Magnitude (Angle) of Boundary Nodes /p.u. (/°)		
		C-PF	MSS-PF	LSI-PF
A	14	1.0253 (-16.4631)	1.0253 (-16.4631)	1.0253 (-16.4631)
B	14	1.0190 (-16.4583)	Diverge	1.0190 (-16.4583)
C	8	1.0050 (-4.9888)	1.0050 (-4.9888)	1.0050 (-4.9888)
	9	0.9806 (-10.0724)	0.9806 (-10.0724)	0.9806 (-10.0724)
	12	1.0148 (-10.8154)	1.0148 (-10.8154)	1.0148 (-10.8154)
	18	1.0034 (-12.4245)	1.0034 (-12.4245)	1.0034 (-12.4245)
D	8	1.0050 (-5.1042)	Diverge	1.0050 (-5.1042)
	9	0.9811 (-10.1886)		0.9811 (-10.1886)
	12	1.0145 (-10.8892)		1.0145 (-10.8892)
	18	1.0029 (-12.5811)		1.0029 (-12.5811)

TABLE II
Iterations and Time Consumptions of I-T&D PF Algorithms

Case	Time Consumptions /ms (Iteration Number)			
	MSS-PF	LSI-PF ($m=2$)	LSI-PF ($m=3$)	LSI-PF ($m=\infty$)
A	125.0 (20)	47.6 (8)	31.2 (6)	34.8 (6)
A2	53.6 (9)	32.6 (6)	29.7 (5)	29.9 (5)
B	Diverge	66.8 (11)	36.4 (7)	38.6 (7)
B2	227.3 (45)	51.6 (9)	36.9 (7)	33.9 (6)
C	250.0 (20)	100.7 (8)	89.0 (7)	95.8 (7)
C2	80.1 (6)	68.9 (5)	71.1 (5)	72.4 (5)
D	Diverge	136.9 (11)	114.7 (9)	100.4 (8)
D2	139.4 (11)	85.8 (7)	86.1 (7)	88.2 (7)

Then, Fig. 4 shows the variation curves of boundary nodal voltage magnitude and angle under Case A and Case B. Fig. 4(a) and Fig. 4(b) show that the LSI-PF converges with a faster convergence rate than the MSS-PF. Fig. 4(c) and Fig. 4(d) show that the LSI-PF can converge within finite iterations even if the MSS-PF diverges.

Citation information: DOI: 10.17775/CSEEJPES.2021.03680, CSEE Journal of Power and Energy Systems

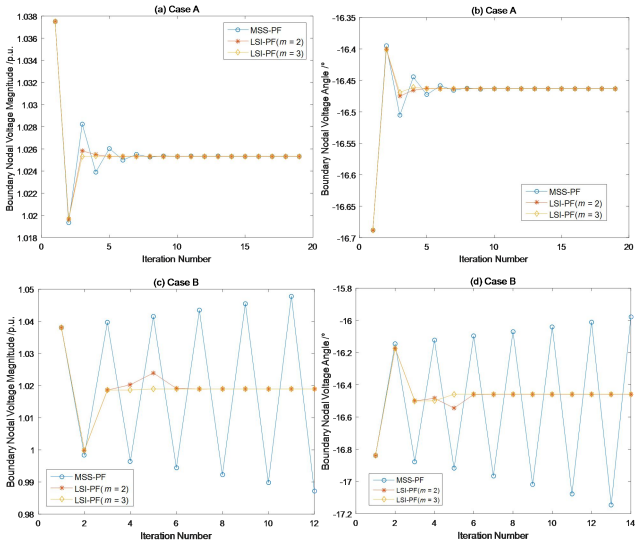

Fig. 4. Variation curves of boundary nodal voltage in I-T&D PF

B. LSI-HGD for I-T&D OPF

The detailed formulation (constraints and objective functions) of the I-T&D OPF applied in this paper is presented in Appendix B of [3]. The objective is to minimize the overall generation costs of an I-T&D system. The cost function of each generator is shown in TABLE B-II, Appendix B. The constraints of I-T&D OPF include i) the power flow constraints; ii) the nodal voltage magnitude and angle constraints; iii) line capacity constraints; iv) generator constraints; v) shunt capacitor constraints.

Three I-T&D OPF methods are investigated: i) Centralized OPF (C-OPF): unrealistic in real-world operation, but it is an accurate model, which can be considered as a benchmark in the test. The algorithm applied in the test is the 'runopf' function in MATPOWER 7.0; ii) conventional HGD [3]; iii) LSI-HGD. The convergence tolerance is set as 1e-6. The flat start is applied for initial value selection, i.e., the initial values of boundary nodal voltage magnitudes are 1 p.u. and the initial values of boundary nodal voltage angles are 0°; the initial values of sthe Lagrange multipliers of boundary power flow equations are 0. The maximum iteration number between TSO and DSOs for ii) and iii) is set as 100.

TABLE III records the boundary voltage magnitudes and objective functions in some cases. It shows that, under Case A and D, the LSI-HGD can achieve the same results as the C-OPF and the HGD. Under Case B, C, and E, the conventional HGD diverges, while the LSI-HGD can still achieve the same results as the C-OPF.

TABLE III
I-T&D OPF RESULTS UNDER DIFFERENT ALGORITHMS

Case	Objective Functions /$ (Voltage Magnitude of Boundary Nodes /p.u.)		
	C-OPF	HGD	LSI-HGD
A	585.59 (1.0360)	585.59 (1.0360)	585.59 (1.0360)
B	581.21 (1.0388)	Diverge	581.21 (1.0388)
C	588.08 (1.0150, 1.0360, 1.0390)	Diverge	588.08 (1.0150, 1.0360, 1.0390)
D	129692 (1.0213)	129692 (1.0213)	129692 (1.0213)
E	129474 (1.0444, 1.0426, 1.0381, 1.0136)	Diverge	129474 (1.0444, 1.0426, 1.0381, 1.0136)

TABLE IV records the iterations and time consumptions under different algorithms. It shows that the LSI-HGD can converge under all cases while the HGD diverges under Case B, C, and E. Further, for Case A and D, the LSI-HGD can improve the convergence rate and take fewer iterations to converge. The selection of m is important for the performance. When m is smaller than 3, more iterations are needed (except for Case E). When m is too large, the matrix may be close to singular which leads to inaccurate results. Also, larger m degrades the convergence rate under Case E.

TABLE IV
ITERATIONS AND TIME CONSUMPTIONS OF I-T&D OPF ALGORITHMS

Case	Time Consumptions /ms (Iteration Number)					
	HGD	LSI-HGD (m = 2)	LSI-HGD (m = 3)	LSI-HGD (m = 4)	LSI-HGD (m = 5)	LSI-HGD (m = ∞)
A	2041 (21)	633 (7)	640 (7)	*	*	*
B	Diverge	1296 (14)	929.3 (10)	*	*	*
C	Diverge	5453 (33)	5174 (30)	4501 (25)	3684 (21)	*
D	1253 (8)	988 (7)	1015 (7)	*	*	*
E	Diverge	2886 (13)	3675 (17)	3599 (17)	5134 (23)	*

* Matrix is close to singular. The results may be inaccurate.

Admittedly, the optimal setting of m is case-dependent, and it could be achieved by a batch of trials in numerical experiments. However, it is time-consuming and unnecessary to tune the best setting m for each case in real-world operations. From a perspective of engineering practicability, the setting of m = 3 could be applied for different systems since the LSI-HGD with m = 3 can successfully achieve solutions with relatively high efficiency.

Then, Fig. 5 shows the variation curves of boundary nodal voltage magnitude under Case A and B. Fig. 5(a) shows that the LSI-HGD converges with a faster convergence rate than the HGD. Fig. 5(b) shows that the LSI-HGD can converge within finite iterations even if the HGD cannot converge.

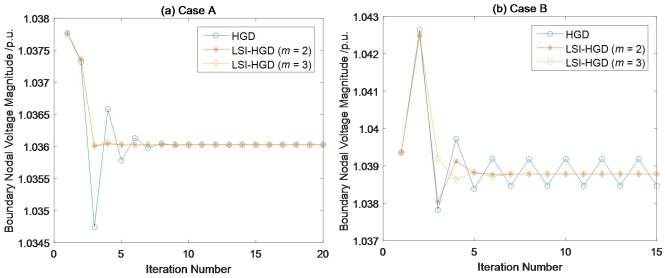

Fig. 5. Variation curves of boundary nodal voltage magnitude in I-T&D OPF

VI. DISCUSSIONS AND EXTENSIONS

A. Discussions about Unbalanced DNs

In real-world operation, the three-phase imbalance in DNs should be considered. Usually, a heterogeneous model could be established for an I-T&D system, where the TN is modeled as single-phase while DNs are modeled as three-phase [2]. Thus, the proposed LSI-PF can be extended into a three-phase form by adding some extra calculations in the boundary part. In specific, for a DN, it is assumed that the three-phase voltage at its root node is symmetric in each iterative step [9]. Also, the boundary power injections for a boundary node are the summation of the power injections of three phases for this node. In this way, there is no significant change in the steps

Citation information: DOI: 10.17775/CSEEJPES.2021.03680, CSEE Journal of Power and Energy Systems

presented in Section IV-A.

B. Nonconvex Nature of AC OPF Models

Due to the nonconvex nature of AC OPF models, it is difficult to guarantee the global optimality of final solutions. However, for optimization problems, even a local optimal solution is meaningful, and [3] points out that enforcing the conventional HGD to I-T&D OPF can still achieve a satisfying accuracy. The proposed LSI-HGD achieves the same accuracy and improves the convergence compared with the conventional HGD. Thus, in practical implementation, the nonconvex nature of AC OPF models will not lead to large deviations.

VII. Conclusions

This paper proposes a LSI-PF for I-T&D PF and a LSI-HGD for I-T&D OPF. Through an extensive demonstration on the test cases, the following observations can be obtained:

- The LSI-PF and LSI-HGD methods can achieve the same accuracy as the methods under the centralized model as well as the conventional MSS and HGD.
- The convergence of the LSI-PF and LSI-HGD is stable, not sensitive to the effects of DNs. To be more specific, for the cases under which the MSS-PF/HGD converges, LSI-PF and LSI-HGD can achieve a better convergence rate; for the cases under which the MSS-PF/HGD diverges, LSI-PF and LSI-HGD can maintain a good convergence.
- The LSI-PF and LSI-HGD with appropriate settings of m usually show higher efficiency, since the convergence is significantly enhanced compared with the MSS-PF and the HGD. A good empirical setting of m is 3, which could be applied to different systems in real-world operations.

In conclusion, the proposed LSI-PF and LSI-HGD can significantly benefit real practice.

Appendix A Proof for Theorem I

Assumption iii) implies that $\|\boldsymbol{f}'(\boldsymbol{x})\| \le c < 1$ holds for all $\boldsymbol{x} \in \boldsymbol{B}(\hat{\rho})$, and thus, $\boldsymbol{g}'(\boldsymbol{x}^*)$ is nonsingular. Denote the Lipschitz constant of $\boldsymbol{g}'$ in $\boldsymbol{B}(\hat{\rho})$ by γ. Thus, Lemma 1 can be established as follows based on Lemma 4.3.1 from [22].

Lemma 1 For sufficiently small $\rho \le \hat{\rho}$ and all $\boldsymbol{x} \in \boldsymbol{B}(\hat{\rho})$,

$$\|\boldsymbol{g}(\boldsymbol{x}) - \boldsymbol{g}'(\boldsymbol{x}^*)\boldsymbol{e}\| \le \frac{\gamma}{2}\|\boldsymbol{e}\|^2 \tag{A–1}$$

$$(1-c)\|\boldsymbol{e}\| \le \|\boldsymbol{g}(\boldsymbol{x})\| \le (1+c)\|\boldsymbol{e}\| \tag{A–2}$$

Then, the proof for Theorem 1 is as follows [23].

First, choose $\rho < \min(2(1-c)/\gamma, \hat{\rho})$ to make (A-3) hold.

$$\frac{c}{\hat{c}} + \frac{M_\alpha \gamma \rho}{2(1-c)}\hat{c}^{-m-1} \le 1 - \frac{\gamma\rho}{2(1-c)} \tag{A–3}$$

Then, choose $\boldsymbol{x}_0$ to make (A-4) hold.

$$\frac{M_\alpha(c+\gamma\rho/2)}{1-c}\hat{c}^{-m}\|\boldsymbol{g}(\boldsymbol{x}_0)\| \le \frac{M_\alpha(1+c)(c+\gamma\rho/2)}{1-c}\hat{c}^{-m}\|\boldsymbol{e}_0\| \le \rho \tag{A–4}$$

Next, prove Theorem 1 by induction.

Assume that for all $0 \le k \le K$ that (A-5) holds for $K = 0$.

$$\|\boldsymbol{g}(\boldsymbol{x}_k)\| \le \hat{c}^k \|\boldsymbol{g}(\boldsymbol{x}_0)\| \tag{A–5}$$

According to Lemma 1, denote

$$\boldsymbol{g}(\boldsymbol{x}_k) = \boldsymbol{g}'(\boldsymbol{x}^*)\boldsymbol{e}_k + \Delta_k, \|\Delta_k\| \le \frac{\gamma}{2}\|\boldsymbol{e}_k\|^2 \tag{A–6}$$

Let,

$$\|\bar{\Delta}_k\| = \frac{1}{2}\sum_{j=0}^{m_K}|\alpha_K^j|\gamma\|\boldsymbol{e}_{K-m_K+j}\|^2 \tag{A–7}$$

Lemma 1 implies that

$$\begin{aligned}\|\boldsymbol{e}_{K-m_K+j}\|^2 &\le \|\boldsymbol{e}_{K-m_K+j}\|(\frac{1}{1-c})\|\boldsymbol{g}(\boldsymbol{x}_{K-m_K+j})\| \\ &\le \frac{\rho}{1-c}\|\boldsymbol{g}(\boldsymbol{x}_{K-m_K+j})\| \le\le \frac{\rho}{1-c}\hat{c}^{K-m}\|\boldsymbol{g}(\boldsymbol{x}_0)\|\end{aligned} \tag{A–8}$$

Thus, according to Assumption iv),

$$\|\bar{\Delta}_k\| \le \frac{M_\alpha\gamma\rho}{2(1-c)}\hat{c}^{K-m}\|\boldsymbol{g}(\boldsymbol{x}_0)\| \le \frac{M_\alpha\gamma\rho}{2(1-c)}\hat{c}^{-m}\|\boldsymbol{g}(\boldsymbol{x}_0)\| \tag{A–9}$$

Since

$$\boldsymbol{e}_{K+1} = \sum_{j=0}^{m_K}(\alpha_j^K \boldsymbol{f}(\boldsymbol{x}^*)\boldsymbol{e}_{K-m_K+j}) + \bar{\Delta}_k \tag{A–10}$$

According to (A-5),

$$\begin{aligned}\|\boldsymbol{e}_{K-m_K+j}\| &\le \frac{1}{1-c}\|\boldsymbol{g}(\boldsymbol{x}_{K-m_K+j})\| \\ &\le \frac{1}{1-c}\hat{c}^{K-m_K+j}\|\boldsymbol{g}(\boldsymbol{x}_0)\| \le \frac{1}{1-c}\hat{c}^{-m}\|\boldsymbol{g}(\boldsymbol{x}_0)\|\end{aligned} \tag{A–11}$$

and thus,

$$\left\|\sum_{j=0}^{m_K}\alpha_j^K(f'(x^*)\boldsymbol{e}_{K-m_K+j})\right\| \le \frac{M_\alpha c}{1-c}\hat{c}^{-m}\|\boldsymbol{g}(\boldsymbol{x}_0)\| \tag{A–12}$$

Thus, with (A-9) and (A-10),

$$\|\boldsymbol{e}_{K+1}\| \le \frac{M_\alpha(c+\gamma\rho/2)}{1-c}\hat{c}^{-m}\|\boldsymbol{g}(\boldsymbol{x}_0)\| \le \rho \tag{A–13}$$

Since

$$\boldsymbol{g}(\boldsymbol{x}_{K+1}) = \boldsymbol{f}'(\boldsymbol{x}^*)\sum_{j=0}^{m_K}\alpha_j^K\boldsymbol{g}(\boldsymbol{x}_{K-m_K+j}) - \bar{\Delta}_K + \Delta_{K+1} \tag{A–14}$$

according to Lemma 1,

$$\|\Delta_{K+1}\| \le \frac{\gamma\rho}{2(1-c)}\|\boldsymbol{g}(\boldsymbol{x}_{K+1})\| \tag{A–15}$$

With (A-5), (A-9), (A-14), and (A-15),

Citation information: DOI: 10.17775/CSEEJPES.2021.03680, CSEE Journal of Power and Energy Systems

$$\begin{aligned}&\left\|\boldsymbol{g}(\boldsymbol{x}_{K+1})\right\|[1-\frac{\gamma\rho}{2(1-c)}]\le\left\|\boldsymbol{g}(\boldsymbol{x}_{K+1})\right\|-\left\|\Delta_{K+1}\right\|\\&\le c\left\|\sum_{j=0}^{m_K}\alpha_j^K\boldsymbol{g}(\boldsymbol{x}_{K-m_K+j})\right\|+\left\|\bar{\Delta}_K\right\|\le c\left\|\boldsymbol{g}(\boldsymbol{x}_K)\right\|+\left\|\bar{\Delta}_K\right\|\quad(\text{A}-16)\\&=[\frac{c}{\hat{c}}+\frac{M_\alpha\gamma\rho}{2(1-c)}\hat{c}^{-m-1}]\hat{c}^{K+1}\left\|\boldsymbol{g}(\boldsymbol{x}_0)\right\|\end{aligned}$$

Thus, with (A-3),

$$\left\|\boldsymbol{g}(\boldsymbol{x}_{K+1})\right\|\le\hat{c}^{K+1}\left\|\boldsymbol{g}(\boldsymbol{x}_0)\right\|\qquad(\text{A}-17)$$

So, (A-5) holds for $k=K+1$.

APPENDIX B CASE INFORMATION

A. I-T&D PF Cases

Several I-T&D cases are constructed, as shown in TABLE B-I. Some DGs are accessed into IEEE case69 to construct case69A and case69B. When they are considered as PV-typed (QV-typed), they have a constant active/reactive power output of 0.5MW/0.5MVar. Each feeder is connected to the TN via a transformer with r = 0.002 p.u., x = 0.01 p.u., and *ratio* = 1.

TABLE B-I
I-T&D PF CASES

Case	TN Case	DN Case	DGs are accessed into Node No. (Control Mode)	DNs are accessed into Bus No.
Case A	case14	case69A	8, 15, 20 (PV)	14
Case A2	case14	case69A	8, 15, 20 (QV)	
Case B	case14	case69B	45, 61 (PV)	
Case B2	case14	case69B	45, 61 (QV)	
Case C	case57	case69A	8, 15, 20 (PV)	8, 9, 12, 18
Case C2	case57	case69A	8, 15, 20 (QV)	
Case D	case57	case69B	45, 61 (PV)	
Case D2	case57	case69B	45, 61 (QV)	

B. I-T&D OPF Cases

Two DN cases are constructed, of which the basic cases are IEEE case69 as shown in TABLE B-II. Several DGs and reactive power compensators (RPCs) are accessed into these cases. The detailed information about DGs and RPCs are also shown in TABLE B-II. The upper and lower limits of the voltage magnitude of all nodes in DNs are 1.1 p.u. and 0.9 p.u.

TABLE B-II
DN CASE INFORMATION

DN Case	Distribution System Cases and Their Modifications							
	Basic Case	Accessed Node No.	Type	Parameters (P/MW, Q/MVar)				Cost Function
				P_{max}	P_{min}	Q_{max}	Q_{min}	
DN1	case69	15, 30	DG	2.0	0	1.0	0	$0.5P^2+P$
DN2	case69	15, 30	DG	2.0	0	1.0	0	$0.5P^2+P$
		45	DG	0.5	0	1.0	0	$0.5P^2+P$
		61	DG	1.0	0	1.0	0	$0.5P^2+P$
		54	RPC	-	-	1.2	0	0

Then, several I-T&D cases are constructed by combining one TN case and one or more DN cases. The detailed case information is shown in TABLE B-III.

TABLE B-III
I-T&D OPF CASES

Case	TN Case	DN Cases	DN(s) is(are) accessed into Bus No.
Case A	case30	DN1	30
Case B	case30	DN2	30
Case C	case30	DN2, DN2, DN2	8, 10, 30
Case D	case118	DN1	118
Case E	case118	DN2, DN2, DN2, DN2	11, 78, 82, 118

REFERENCES

[1] H. Jain, K. Rahimi, A. Tbaileh, R. P. Broadwater, Akshay Kumar Jain and M. Dilek, "Integrated transmission & distribution system modeling and analysis: Need & advantages," *2016 IEEE Power and Energy Society General Meeting (PESGM)*, Boston, MA, 2016, pp. 1-5.

[2] H. Sun, Q. Guo, B. Zhang, Y. Guo, Z. Li and J. Wang, "Master–Slave-Splitting Based Distributed Global Power Flow Method for Integrated Transmission and Distribution Analysis," *IEEE Trans. Smart Grid*, vol. 6, no. 3, pp. 1484-1492, May 2015.

[3] Z. Li, Q. Guo, H. Sun and J. Wang, "Coordinated Transmission and Distribution AC Optimal Power Flow," *IEEE Trans. Smart Grid*, vol. 9, no. 2, pp. 1228-1240, Mar. 2018.

[4] E. Rivero, D. Six and H. Gerard, "Basic schemes for TSO-DSO coordination and ancillary services provision," EU Horizon 2020 SmartNet Project, Dec. 2016. [Online]. Available: https://smartgrids.no/wp-content/uploads/sites/4/2016/01/ISGAN-TSO-DSO-interaction.pdf

[5] A. Zegers and H. Brunner, "TSO-DSO interaction: An overview of current interaction between transmission and distribution system operators and an assessment of their cooperation in smart grids," Int. Smart Grid Action Netw. Discussion Paper, Sep. 2014. [Online]. Available: http://www.ieaisgan.org/index.php?r = home&c = 5/378

[6] ENTSO (European Network of Transmission System Operators), "General guidelines for reinforcing the cooperation between TSOs and DSOs," Nov. 9, 2015. [Online]. Available: https://www.entsoe.eu/Documents/Publications/Position%20papers%20and%20reports/entsoe_pp_TSO-DSO_web.pdf#search = tso%2Ddso

[7] Z. Li, H. Sun, Q. Guo, J. Wang and G. Liu, "Generalized Master–Slave-Splitting Method and Application to Transmission–Distribution Coordinated Energy Management," *IEEE Trans. Power Syst.*, vol. 34, no. 6, pp. 5169-5183, Nov. 2019.

[8] Q. Huang and V. Vittal, "Integrated Transmission and Distribution System Power Flow and Dynamic Simulation Using Mixed Three-Sequence/Three-Phase Modeling," *IEEE Trans. Power Syst*, vol. 32, no. 5, pp. 3704-3714, Sept. 2017.

[9] K. Tang, S. Dong and Y. Song, "Successive-Intersection-Approximation-Based Power Flow Method for Integrated Transmission and Distribution Networks," *IEEE Trans. Power Syst.*, vol. 35, no. 6, pp. 4836-4846, Nov. 2020.

[10] K. Tang, S. Dong, C. Zhu and Y. Song, "Affine Arithmetic-Based Coordinated Interval Power Flow of Integrated Transmission and Distribution Networks," *IEEE Trans. Smart Grid*, vol. 11, no. 5, pp. 4116-4132, Sept. 2020.

[11] Z. Li, J. Wang, H. Sun and Q. Guo, "Transmission Contingency Analysis Based on Integrated Transmission and Distribution Power Flow in Smart Grid," *IEEE Trans. Power Syst.*, vol. 30, no. 6, pp. 3356-3367, Nov. 2015.

[12] Z. Li, J. Wang, H. Sun and Q. Guo, "Transmission Contingency Screening Considering Impacts of Distribution Grids," *IEEE Trans. Power Syst.*, vol. 31, no. 2, pp. 1659-1660, March 2016.

[13] K. Tang, S. Dong, J. Huang and X. Ma, "Operational risk assessment for integrated transmission and distribution networks," *CSEE Journal of Power and Energy Systems*, Early access.

[14] N. G. Singhal and K. W. Hedman, "Iterative transmission and distribution optimal power flow framework for enhanced utilisation of distributed resources," *IET Gener., Transm. Dis.*, vol. 9, no. 11, pp. 1089-1095.

[15] K. Tang, S. Dong, X. Ma, L. Lv and Y. Song, "Chance-Constrained Optimal Power Flow of Integrated Transmission and Distribution Networks with Limited Information Interaction," *IEEE Trans. Smart Grid*, Early access.

[16] A. Mohammadi, M. Mehrtash and A. Kargarian, "Diagonal Quadratic Approximation for Decentralized Collaborative TSO+DSO Optimal Power Flow," *IEEE Trans. on Smart Grid*, vol. 10, no. 3, pp. 2358-2370, May 2019.

[17] K. Tang, S. Dong, J. Cui, Y. Li and Y. Song, "Synthesised-objective collaborative model and its solution algorithm for transmission–distribution coordinated optimisation," *IET Gener. Transm. Dis.*, vol. 14, no. 5, pp. 752-761, Mar. 2020.

[18] A. Krasnosel'skii, "Two remarks on the method of successive approximations," *Uspekhi Matematicheskikh Nauk*, vol. 10, no. 1, pp. 123-127, 1955.

[19] R. Mann, "Mean value methods in iteration," *Proceedings of the American Mathematical Society*, vol. 4, no. 3, pp. 506-510, 1953.

[20] D. Zhang, S. Miao, C. Li, Z. Zheng, W. Yang, J. Han and Y. Li, "A novel once-data-exchange method for solving transmission and distribution networks coordinated ACOPF model," *International Journal of Electrical Power & Energy Systems*, vol. 123, Dec. 2020.

[21] C. Lin, W. Wu, M. Shahidehpour, Y. Guo and B. Wang, "A Non-Iterative Decoupled Solution of the Coordinated Robust OPF in Transmission and Distribution Networks With Variable Generating Units," IEEE Transactions on Sustainable Energy, vol. 11, no. 3, pp. 1579-1588, July 2020, doi: 10.1109/TSTE.2019.2931908.

[22] C. T. Lelley and Z. Q. Xue, "Iterative Methods for Linear and Nonlinear Equations, " no. 16 in Frontiers in Applied Mathematics, SIAM, Philadelphia, 1995.

[23] H. F. Walker and P. Ni, "Anderson Acceleration for Fixed-Point Iterations," *SIAM Journal on Numerical Analysis*, vol. 49, no. 4, pp. 1715–1735, Aug. 2011.